Integrating time-series InSar and ensemble learning model for land subsidence susceptibility mapping

Shuai Li[a,b,c], Lin Zhu[a,b,c], Huili Gong[a,b,c], Xiaojuan Li[a,b,c], Ning Zhang[a,b,c], Xiangyu Meng[a,b,c]

[a] *College of Resource Environment and Tourism, Capital Normal University, Beijing, China*
[b] *Beijing Laboratory of Water Resources Security, Capital Normal University, Beijing, China*
[c] *State Key Laboratory Incubation Base of Urban Environmental Processes and Digital Simulation, Capital Normal University, Beijing, China*
E-mail: Lin Zhu (lin.zhu@cnu.edu.cn)

Abstract: Land subsidence susceptibility mapping (LSSM), which identifies areas with different levels of risk, is important for subsidence control and early warning. The XGBoost model is an ensemble learning model that can effectively enhance simulation accuracy and is suitable for LSSM. Due to long-term over-exploitation of groundwater, severe land subsidence has occurred in the Beijing Plain, which was selected as the study area. Firstly, Synthetic Aperture Radar (SAR) images from 2015 to 2023 were processed using time-series Interferometric Synthetic Aperture Radar (InSAR) technology to obtain regional displacement information. Secondly, the main influencing factors of LSS include the rate of groundwater level (GWL) change in the first and second confined aquifers, the thickness of compressible layers, the static load of buildings, and the drainage density. The XGBoost model, combined with these factors, was used to map the LSS in the study area from 2015 to 2023. The SHapley Additive exPlanations (SHAP) model was used to analyse the contribution rates of the input factors. Finally, based on the predicted GWLs from 2023 to 2035, the distribution pattern of LSS was assessed. Meanwhile, the GWL threshold for the region, which transfers from the Very High risk area to the Low risk area was determined. The results show that the Area Under the Curve (AUC) value of the training set is 0.94, and that of the validation set is 0.83. Both are above 0.8, which reflects that the XGBoost model has high classification accuracy and can effectively map LSS. The results of the SHAP interpretability analysis show that the GWL change of the second confined aquifer has the greatest contribution rate to LSS (with a SHAP value of 0.36), while the drainage density has the smallest contribution rate (with a SHAP value of 0.07). Compared with the period from 2015 to 2023, the areas with High risk and Very High risk levels would disappear during 2023-2035. By identifying the regions that transfer from Very High to Low and overlaying the GWLs of the second confined aquifer in 2023 and 2035, it is found that when the GWL rises by 10 m, the risk level of LSS can be effectively mitigated. The research provides technical support for the assessment and prevention of geological disasters.

Keywords: *Land subsidence susceptibility mapping, Ensemble learning, Time-series InSAR, Interpretability, Geostatistical analysis*

1. INTRODUCTION

Land subsidence is a slow-onset geohazard characterised by a gradual decline in ground elevation. Excessive groundwater extraction often triggers land subsidence accompanied by ground fissures, posing constraints on sustainable economic and social development (Ao, 2024). Land Subsidence Susceptibility Mapping (LSSM) mitigates these risks by selecting key risk factors, classifying risk levels, and formulating response strategies, thereby effectively reducing geologic hazards caused by land subsidence (He et al., 2025). However, relying on a single modelling approach may introduce uncertainty due to parameter sensitivity and limited generalizability (Hosseinzadeh et al., 2024).

Ensemble learning models, which combine predictions from multiple base learners, can effectively reduce variance and bias, thereby improving predictive accuracy (Yananto et al., 2024). Yu et al. (2025) used XGBoost, LightGBM, and CatBoost models to assess land subsidence susceptibility in Hangzhou, China. Beijing is one of the few megacities worldwide that relies primarily on groundwater for its municipal supply (Zhu et al., 2020). Long-term over-extraction has produced multiple groundwater level (GWL) decline funnels and induced severe subsidence, with a historical maximum rate of 159 mm/yr. Conducting an assessment of the LSS for the Beijing Plain can enable the determination of the risk level and prevent further development of disasters. It can also provide research cases for other cities and regions.

Therefore, we employed time-series InSAR techniques to obtain vertical deformation rates across the Beijing Plain, China, using Sentinel-1A/B data from 2015 to 2023. The influencing factors of land subsidence, such as the GWL change of the confined aquifer, lithology, static load of buildings, and drainage density, were selected. The

XGBoost model was used to map the LSS in the study area from 2015 to 2023. The ROC curve was used to verify the accuracy, and SHapley Additive exPlanations (SHAP) method was used to explore the interpretability of models (Ye et al., 2024). Finally, the distribution pattern of LSSM in Beijing from 2023 to 2035 was predicted and the GWL threshold for mitigating the risk of LSS has been identified. This study provides a technical basis for improving urban subsidence risk management.

2. STUDY AREA AND DATASETS

2.1. Study Area

Beijing, the capital of China, is situated in the northwestern part of the North China Plain (115°25′–117°30′E, 39°26′–41°03′N), covering 6,390 km^2 with nearly 22 million residents in 2023 (Figure 1). It has a typical temperate continental monsoon climate, with an average annual precipitation of 529 mm from 1991 to 2023. From 1999 to 2008, there was a continuous drought with an average annual precipitation of 480 mm. To meet the water demand during this period, groundwater became the main water supply source, providing almost two-thirds of the water needs. This caused the average depth of the GWL to decrease by 8.68 m in the unconfined aquifer, forming a regional piezometric depression cone. The South-to-North Water Diversion Project (SNWDP), which has been in operation since December 2014, has helped alleviate water shortages in the area by delivering 9 billion m^3 of water to Beijing by 2023. Consequently, the GWL has risen by approximately 11 m from 2015 to 2023 (Authority, 2023).

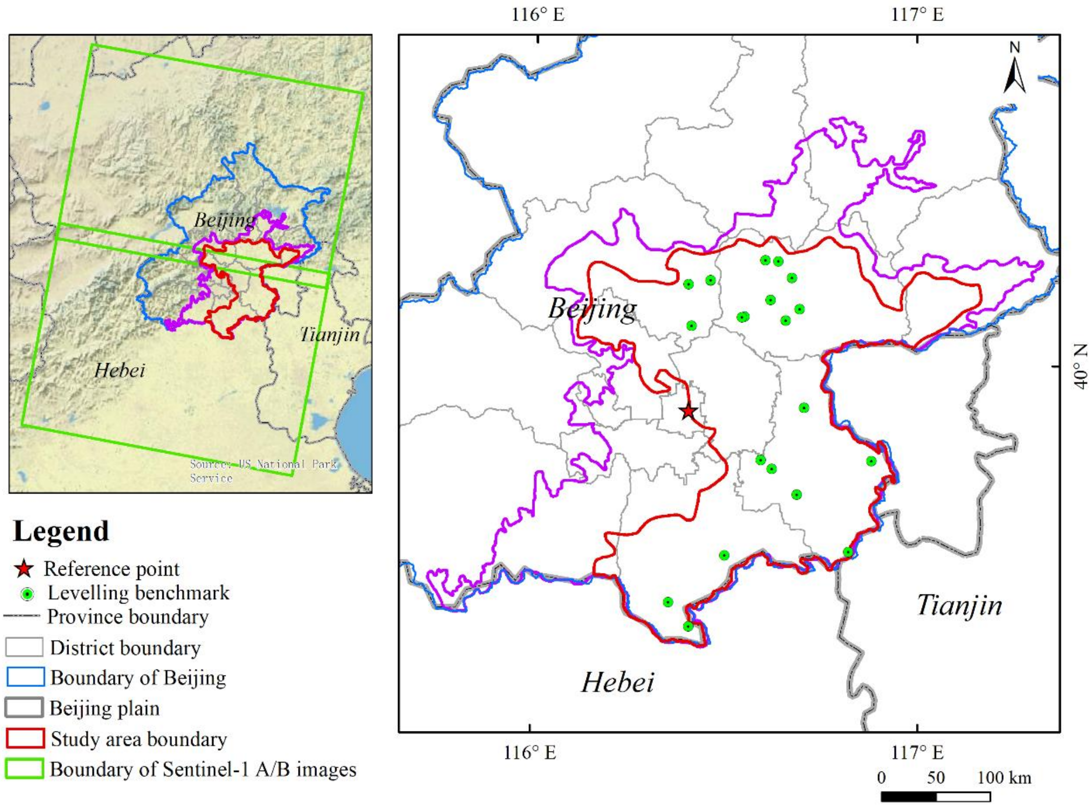

Figure 1 Study area

The complex aquifer system transitions gradationally from a single aquifer in the northwest to multiple aquifers in the southeast across the Beijing Plain. Quaternary sediments are widely distributed and vertically categorised into four aquifers. Among them, the first aquifer is the unconfined aquifer, while the second to fourth aquifers are confined aquifers (Table 1). According to the studies by Chen et al. (2020), the primary cause of land subsidence in the Beijing Plain is the excessive extraction of groundwater from confined aquifers. Among these, the first and second confined aquifers show a strong correlation between GWL distribution and subsidence patterns. Specifically, the location of the maximum depression funnel in the second confined aquifer corresponds spatially to the most severe subsidence funnel within the plain (Cao et al., 2022). Therefore, this study defines the boundaries of the second confined aquifer group as the research area for subsequent research.

Table 1 Division of the aquifer groups in the Beijing Plain

Aquifer group	Major lithology	Depth of the bottom
Unconfined aquifer	Silt, silty sand, and sandy clay	0-50 m
First confined aquifer	Multiple types of gravel, sand, and clay soil	50-100 m
Second confined aquifer	Multiple types of gravel, sand, and clay soil	100-180 m
Third confined aquifer	Mainly sand	>180 m

2.2. Data Sets

2.2.1 SAR data

A total of 134 scenes of descending Sentinel-1A/B data covering the study area (from December 19, 2014, to December 27, 2023) were collected to monitor deformation in the study area.

2.2.2 Levelling measurement data

To verify the deformation monitoring results of InSAR, data from 28 levelling points located in the Beijing Plain area from 2015 to 2022 were collected, and their locations are shown in Figure 1.

2.2.3 Impact factor

The primary geological condition for land subsidence in the study area is the extensive compressible soil. The main external factor is the long-term over-extraction of groundwater, especially in the confined aquifers. Additionally, static load from buildings and the drainage density also influence the occurrence and development of land subsidence in the study area (Arabameri et al., 2020). Therefore, five land subsidence influencing factors were selected for evaluating LSS (Figure 2): the GWL change rate of the first confined aquifer is shortened to ‘CA1’, the GWL change rate of the second confined aquifer is shortened to ‘CA2’, the index-based built-up index change rate is shortened for ‘IBI’ (Zhou et al., 2019), compressible layer thickness is shortened to ‘COM’, and drainage density is shortened to ‘DD’.

In this paper, the study area encompasses major subsidence zones in Beijing, including Chaoyang District, Shunyi District, and Tongzhou District. The region was discretised into 500 m × 500 m grid cells, yielding a total of 14,958 spatial units from 2015 to 2023. Through randomised sampling, 80% of the grids (11,966 cells) were designated as the training dataset, with the remaining 20% (2,992 cells) reserved for validation.

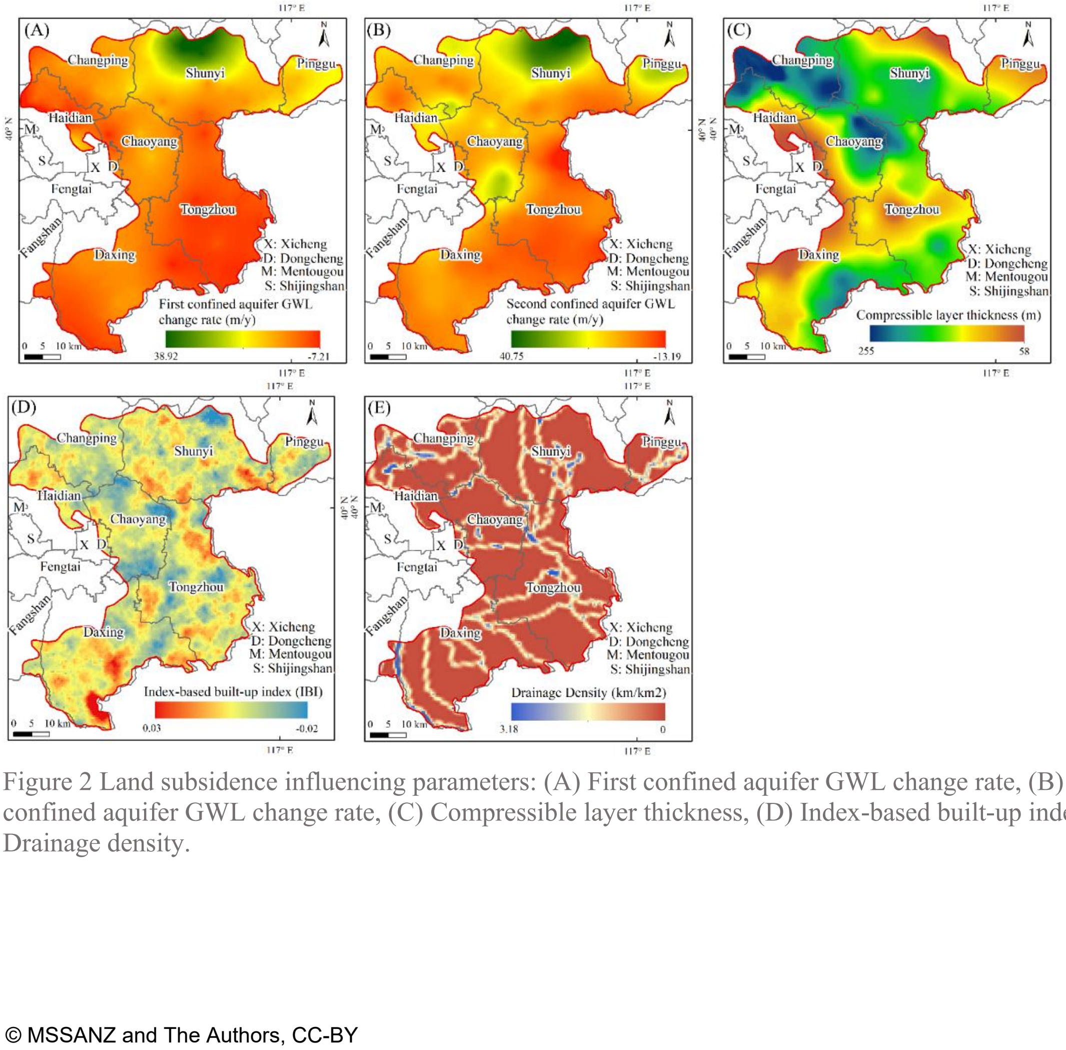

Figure 2 Land subsidence influencing parameters: (A) First confined aquifer GWL change rate, (B) Second confined aquifer GWL change rate, (C) Compressible layer thickness, (D) Index-based built-up index, (E) Drainage density.

3. METHODOLOGY

This work employs time-series InSAR techniques and ensemble learning models to map LSS in the Beijing Plain, analyze differences in LSS distribution, and determine the contribution rate of input factors. The distribution pattern of LSS in the study area was predicted, and the GWL threshold for mitigating the risk of LSS has been identified.

3.1. Persistent Scatterer InSAR (PS-InSAR) technology

The fundamental principle of InSAR technology involves extracting Line-of-Sight (LOS) deformation information from interferograms generated by two SAR images acquired at different times over the same region. These interferograms are composed of distinct phase components (Ferretti et al., 2002):

$$\Delta\varphi = \varphi_{def} + \varphi_{topo} + \varphi_{orb} + \varphi_{atm} + \varphi_{noise} \tag{1}$$

Where, φ_{def} is the deformation phase along the line of sight (LOS), φ_{topo} is the topographic phase, φ_{orb} is the orbital error phase, φ_{atm} is the phase component due to atmospheric delay, and φ_{noise} is the phase noise.

$$D_v = \frac{\lambda \cdot \varphi_{def}}{4 \cdot \pi \cdot \cos(\theta)} \tag{2}$$

Where, λ represents the radar wavelength, θ denotes the radar incidence angle, and D_v denotes for the vertical deformation.

3.2. Ensemble Learning Model

The XGBoost (eXtreme Gradient Boosting) algorithm, proposed by Chen in 2016, is an advanced ensemble method integrating two core components: (1) Additive Modelling: The strong learner is constructed through linear aggregation of weak learners. (2) Forward Stagewise Optimisation: The new learner generated in the next round of iteration is trained based on the previous round's results. The base learner of the XGBoost algorithm is the decision tree. The results of all decision trees are added together as the final output of the model. The calculation formula is as follows:

$$\hat{y}_i = \sum_{p=1}^{P} f_p(W_i), f_p \in F \tag{3}$$

Among them, $\hat{y}_i$ represents the predicted classification value of the i-th land subsidence susceptibility, f_p represents the p-th decision tree, P represents the total number of decision trees, F represents the set of all decision trees, and W_i represents the i -th input sample set.

3.3. SHAP method

As a game theory-based interpretability method for machine learning models, SHAP has the following advantages: it can quantify the contribution of each feature to the model output; it can characterise the direction of the feature's influence (positive contribution or negative contribution); and it can explain the interaction effects between features.

$$S_{ij} = \sum_{Q \in N \backslash \{j\}} \frac{q!\,(n-q-1)!}{n!} \left[\hat{y}_i\left(w_i^{Q \cup \{j\}}\right) - \hat{y}_i\left(w_i^{Q}\right)\right] \tag{4}$$

Where: S_{ij} represents the SHAP value between the LSS y_i of the i-th time-series PS point and the j-th influencing factor w_{ij}; N denotes the set of all influencing factors, with a total of n influencing factors; Q represents a subset composed of some influencing factors (at least one) in set N; q is the number of influencing factors contained in Q; and $Q \in N$. $\hat{y}_i\left(w_i^{Q}\right)$ stands for the predicted land subsidence rate of the i -th PS time-series point obtained by the model constructed using the influencing factors in Q without adding factor j; ŷ_i $\hat{y}_i\left(w_i^{Q \cup \{j\}}\right)$ represents the predicted value obtained by the corresponding model after adding factor j.

4. RESULTS

4.1. Deformation results of PS-InSAR

The levelling benchmark data were applied to validate the derived land subsidence through InSAR technology. The correlation coefficient between the levelling benchmarks data and the vertical displacement derived from SAR images was 0.94 (Figure 3A). The maximum displacement rate in the study area was −80 mm/yr from 2015 to 2023, which was located in Jinzhan, Chaoyang District and denoted with a triangle on Figure 3B.

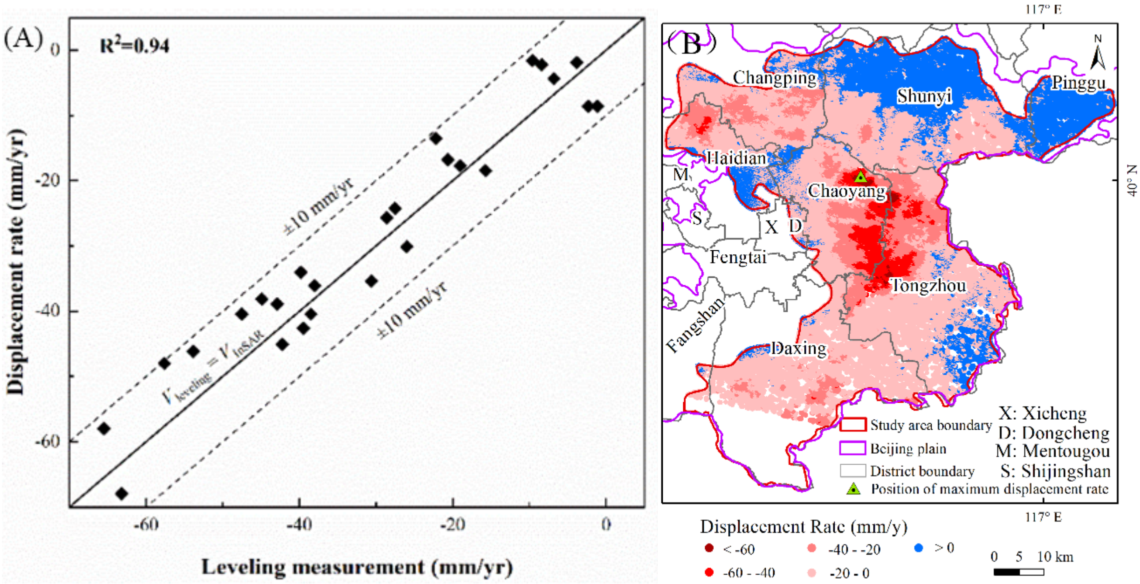

Figure 3 Comparison of subsidence from the levelling benchmarks data and InSAR results (A); Average vertical displacement rates obtained by the InSAR techniques in the study area (B).

4.2. Land subsidence susceptibility map

The hyperparameter settings of the XGBoost model are shown in Table 2. The LSSM was classified into five categories based on displacement rates: Rebound (>0 mm/yr), Low (0 mm/yr ~ -20 mm/yr), Medium (-20 mm/yr ~ -40 mm/yr), High (-40 mm/yr ~ -60 mm/yr), and Very High (<-60 mm/yr). The proportion of areas classified as Very High risk by the XGBoost model was 0.37% (Table 3) and distributed only in the Chaoyang-Tongzhou District (Figure 4A).

The performance of the model was evaluated by the ROC curve. The results showed that the AUC on the training set was 0.94, and the AUC on the validation set was 0.83 (Figure 4B). This indicated that the classification results of the XGBoost model were of high accuracy.

The results of SHAP interpretability analysis show that the rate of GWL change in the second confined aquifer has the largest contribution (0.36), followed by the rate of GWL change in the first confined aquifer and the thickness of the compressible layer (0.34 and 0.27 respectively), while the rate of change in building static load and river network density have the smallest contribution rates (0.09 and 0.07 respectively).

Table 2 Hyper-parameter setting in XGBoost model

Hyper-parameter	n_estimators	max_depth	learning_rate	num_class	subsample	tree_method
Value	100	6	0.1	5	0.8	0.8

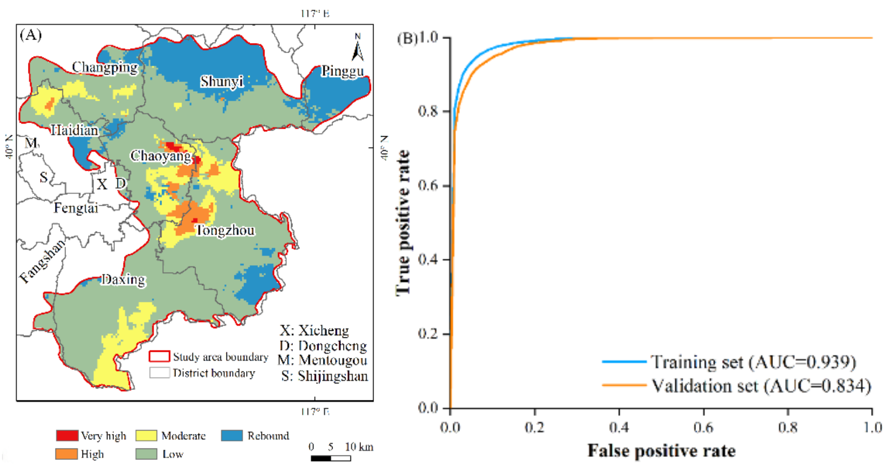

Figure 4 LSSM from 2015 to 2023 by using XGBoost model (A); ROCs of XGBoost model for the training sets and validation set (B).

Table 3 Percentage of susceptibility classes in XGBoost models

Class	Rebound	Low	Moderate	High	Very high
Area proportion	19.79 %	65.21 %	11.54 %	3.09 %	0.37 %

4.3. Prediction of LSS

Considering that the GWL change was an important factor affecting LSS, a numerical model combined with the SSP126 scenario data from CMIP6 was used to predict the GWLs of the first and second confined aquifers in the study area in 2035. Among them, based on the hydrogeological conditions of the study area, the groundwater flow system exhibits heterogeneous, isotropic, and unsteady. The selection of SSP119 is based on its goal of limiting global warming to a level slightly above the pre-industrial era, which enables it to provide effective support for the formulation of long-term climate policies. With the other 3 influencing factors maintaining a constant change rate, the trained XGBoost model was applied to predict the future distribution pattern of LSS in the study area.

The results showed that the GWLs of both the first and second confined aquifers would rise to varying degrees from 2023 to 2035, which led to a slowing pattern of LSS (Figure 5). Among them, the area proportion of the Low grade was about 88%, and that of the Moderate grade was about 12%. SSP126 was a low-emission scenario, which indicated that even if there was no significant increasing trend in precipitation in the future, the risk of land subsidence susceptibility in the study area would still decrease.

Furthermore, by calculating the transition matrix, the Very High risk regions in the LSSM from 2015 to 2023 that transfer into Low regions from 2023 to 2035 (referred to as ‘Transfer regions’) were identified. Considering that the GWL change of the second confined aquifer has the greatest contribution rate to LSS, the GWL map of the second confined aquifer in 2023 and 2035 were overlaid to identify the GWL threshold (Figure 5D-E). The results show that the GWL of the Transfer regions is between -20 m and -10 m in 2023, while it ranges from -15 to 5 m in 2035. This indicates that when the average rising amplitude of the GWL in the second confined aquifer reaches 10 m, the risk level of LSS can be effectively reduced.

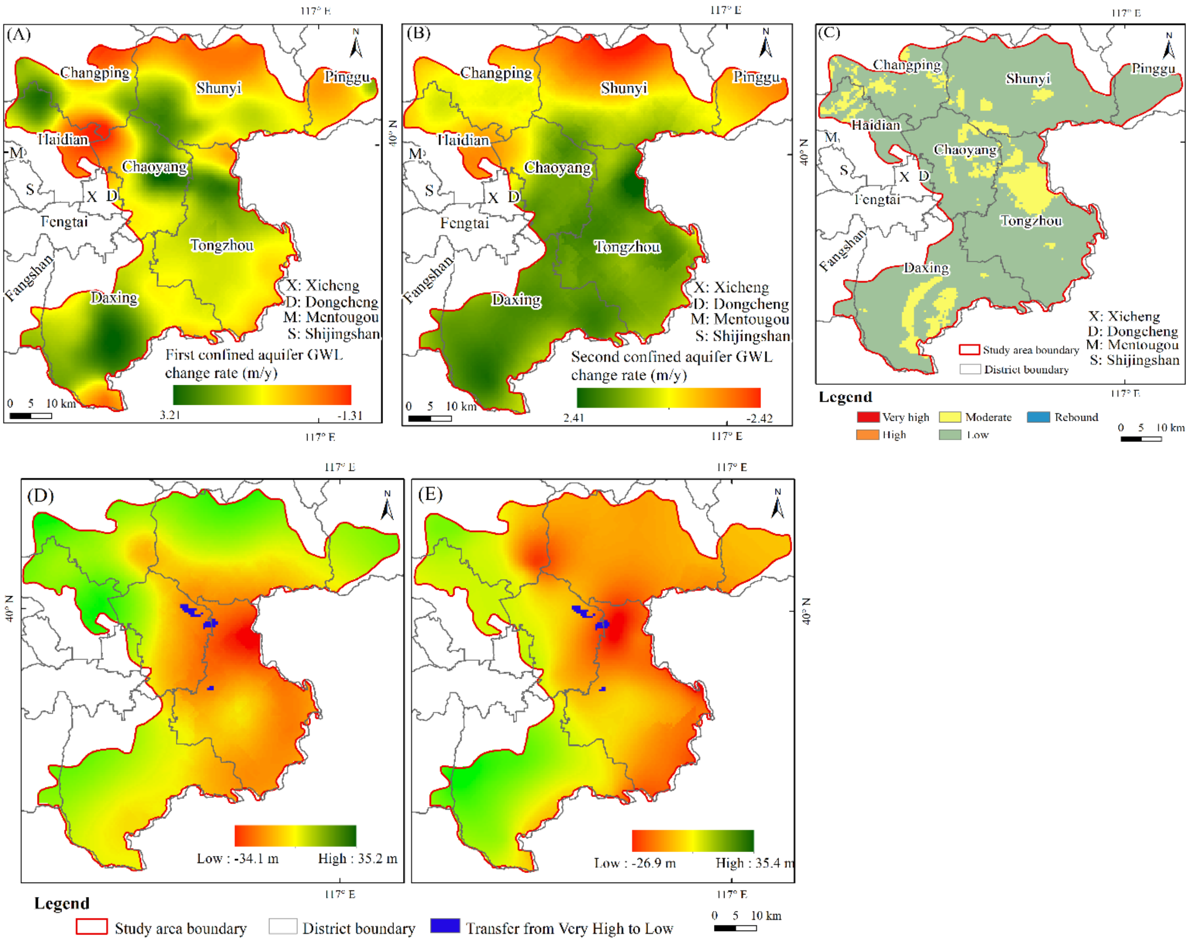

Figure 5 First confined aquifer GWL change rate from 2023 to 2035 (A); Second confined aquifer GWL change rate from 2023 to 2035 (B); LSSM from 2023 to 2035 (C); GWL overlaid onto the transfer regions in 2023 (D); GWL overlaid onto the transfer regions in 2035 (E).

5. CONCLUSION

In this study, the PS-InSAR technology was used to obtain the time series monitoring data of ground subsidence in the Beijing Plain from 2015 to 2023. Subsequently, the LSS distribution of the study area was mapped using XGBoost, and the model was evaluated. Finally, the future distribution pattern of LSS was predicted. The main findings are as follows:

- From 2015 to 2023, the maximum displacement point was located in Jinzhan Township, Chaoyang District.
- For the performance of XGBoost, the AUC on the training set was 0.939, and that on the validation set was 0.834. The interpretable results indicate that the change in the GWL of the second confined aquifer is the main contributing factor (with a SHAP value of 0.36).
- The GWLs of both the first and second confined aquifers would rise to varying degrees from 2023 to 2035, which led to a slowing pattern of LSS. By identifying the Transfer regions from the Very High risk area to the Low-risk area, and overlaying the GWLs of the second confined aquifer in 2023 and 2035, it was found that when the GWL rises by 10 m, the risk level of LSS can be effectively reduced.

ACKNOWLEDGEMENTS

This work was supported by the National Natural Science Foundation of China (No. 42271082); Collaborative project between the Ministry of Natural Resources and Tianjin Province (No. 2024ZRBSHZ011).

REFERENCES

Ao, Z.H., Xiaomei; Tao, Shengli; et al., 2024. A national-scale assessment of land subsidence in China’s major cities. Science 384, 301-306.

Arabameri, A., Saha, S., Roy, J., Tiefenbacher, J.P., Cerda, A., Biggs, T., Pradhan, B., Thi Ngo, P.T., Collins, A.L., 2020. A novel ensemble computational intelligence approach for the spatial prediction of land subsidence susceptibility. Science of The Total Environment 726.

Authority, B.W., 2023. Beijing Water Resources Bulletin (2023).

Cao, X., Zhu, L., Gong, H., Guo, L., Wei, Y., Guo, T., Chen, B., Wang, H., Li, H., 2022. Land subsidence simulation in the east of Beijing plain based on the AM-LSTM Network. National Remote Sensing Bulletin 26.

Chen, B., Gong, H., Chen, Y., Li, X., Zhou, C., Lei, K., Zhu, L., Duan, L., Zhao, X., 2020. Land subsidence and its relation with groundwater aquifers in Beijing Plain of China. Science of The Total Environment 735.

Chen, T., 2016. Story and lessons behind the evolution of XGBoost.

Ferretti, A., Prati, C., Rocca, F., 2002. Permanent scatterers in SAR interferometry. IEEE Transactions on geoscience and remote sensing 39, 0196-2892.

He, Y., Gao, B., Yan, H., Zhang, Q., Zhang, L., Li, W., He, X., Lu, J., 2025. DBPFNet: a double branch parallel fusion neural network method for land subsidence susceptibility mapping with InSAR observation data. International Journal of Digital Earth 18, 1753-8947.

Hosseinzadeh, E., Anamaghi, S., Behboudian, M., Kalantari, Z., 2024. Evaluating Machine Learning-Based Approaches in Land Subsidence Susceptibility Mapping. Land 13, 2073-2445X.

Yananto, A., Yulianto, F., Wibowo, M., Rahili, N., Husada Fadjar Perdana, D., Wiguna, E.A., Prabowo, Y., Iswari, M.Y., Ma’rufatin, A., Fachrudin, I., 2024. Integration Sentinel-1 SAR data and machine learning for land subsidence in-depth analysis in the North Coast of Central Java, Indonesia. Earth Science Informatics 17, 4707-4738.

Ye, M., Zhu, L., Liu, X., Huang, Y., Chen, B., Li, H., 2024. Soil organic matter content inversion using continuous wavelet transform, SHAP and XGBoost. Environmental Science 45(04):2280-2291.

Yu, B., Xing, H., Ge, W. et al. Explainable machine learning-based land subsidence susceptibility mapping: from feature importance to individual model contributions in ensembled system. Earth Sci Inform 18, 407 (2025). https://doi.org/10.1007/s12145-025-01915-9.

Zhou, C., Gong, H., Chen, B., Li, X., Li, J., Wang, X., Gao, M., Si, Y., Guo, L., Shi, M., Duan, G., 2019. Quantifying the contribution of multiple factors to land subsidence in the Beijing Plain, China with machine learning technology. Geomorphology 335, 48-61.

Zhu, L., Franceschini, A., Gong, H., Ferronato, M., Dai, Z., Ke, Y., Pan, Y., Li, X., Wang, R., Teatini, P., 2020. The 3-D Facies and Geomechanical Modeling of Land Subsidence in the Chaobai Plain, Beijing. Water Resources Research 56.

